# Pulsed phonon lasing in trapped ions

Y. Xie,[1,2] W. Wan,[1,2] H. Y. Wu,[1,2] F. Zhou,[1] L. Chen,[1,*] and M. Feng[1,†]

[1]*State Key Laboratory of Magnetic Resonance and Atomic and Molecular Physics, Wuhan Institute of Physics and Mathematics, Chinese Academy of Sciences, Wuhan 430071, China*

[2]*University of the Chinese Academy of Sciences, Beijing 100049, China*

(Received 28 March 2013; published 6 May 2013)

Optical laser pulses play important roles in various fields, and the phononlike analog, i.e., phonon laser pulses, should also be very useful. We show the possibility of pulsed phonon lasing in trapped ions based on our observation that coherent phonon pulses are generated and then transferred between transverse dimensions due to nonlinear resonance once the oscillation amplitude of the trapped ions is larger than a threshold. We study the pulsed phonon output with the multiple-scale method using the first-order nonlinear differential equations which govern time evolution of the amplitudes and phases of the interacting modes. We also discuss the feasibility of $Q$-switched pulsed phonon lasing and the potential application.

DOI: 10.1103/PhysRevA.87.053402 PACS number(s): 37.10.Vz, 05.45.−a, 32.80.Wr, 37.10.Ty

## I. INTRODUCTION

Phonon lasers, which provide the source of coherent acoustic radiation as an analog to optical lasers, are of great significance in physics. Relevant theoretical analyses have been carried out in several different systems, e.g., trapped ions [1], nanomechanics [2], nanomagnets [3], and quantum dots [4], where coherent amplification of phonons, instead of phonon lasers, was mentioned. Coherent emission of sound waves has also been demonstrated experimentally in microcavity systems [5] and in doped superlattice complexes [6].

The coherent amplification of the phonons from trapped ions, in which the oscillation of a single trapped ion is stimulated in the axial dimension by a blue detuned laser, has been investigated both theoretically and experimentally [7,8]. Based on the amplified phonons, an injection locking has been achieved in the trapped-ion system [9], and such an idea can be applied to detecting ultraweak oscillation forces [10]. Since such models [7–9] are established on a single trapped ion in a single dimension, it is not clear how the generated phonons are outputted, although the $Q$ factor of the system can be adjusted in principle. The phonon lasing based on coupled modes of vibrations has recently been demonstrated in an electromechanical resonator [11].

In this paper, we demonstrate the observation of pulsed phonon lasing in an array of trapped ions, where the phonons are generated in a certain dimension and outputted coherently to another dimension once the oscillation amplitude of the ions exceeds the threshold. To this end, we will consider the generation of phonons in transverse modes (along $x$ and $y$ axes) instead of the longitudinal mode (along the $z$ axis). The key point of our work is the intradimensional coupling due to the nonlinearity in the trap, such as anharmonic potentials [12]. To simplify the problem, we only focus on the center-of-mass (COM) mode of the trapped ions, by which we may neglect the phonon-phonon interaction due to Coulomb nonlinearity [13,14]. As a result, we will show the observation of the pulsed phonons transmitted to another dimension only due to trap potential nonlinearity. Moreover, we discuss the possibility of $Q$-switched pulsed phonon lasing based on elaborate control of the trapped ions.

## II. THE EXPERIMENTAL SETUP AND THE MECHANISM OF PULSED PHONON LASING

Pulsed phonon lasing is observed in our homebuilt linear ion trap [15] (see Fig. 1), where a radiofrequency (rf) voltage of the frequency $\Omega/2\pi = 20$ MHz is applied on the bladelike rf electrodes, and a dc voltage $U_{\rm ec} = 30$ V is applied on the endcap electrodes. The secular motion frequencies are measured to be about $\omega_x/2\pi = 1.103$ MHz, $\omega_y/2\pi = 1.104$ MHz, and $\omega_z/2\pi = 0.264$ MHz for the three dimensions, respectively. For our purpose, we have to first accomplish Doppler cooling using a red-detuned 397 nm cooling laser and a resonant 866-nm repumping laser. Both of the lasers are locked to an iodine stabilized He-Ne laser by transfer cavity technology, leading to a long time drift of less than 2 MHz/h. Throughout this work, the lasers irradiate along the direction $\hat{\mathbf{k}} = (-0.37, 0.03, 0.93)$.

In contrast to the situation in [8], the trapped ions in our case are cooled in both the $x$ axis and the $z$ axis but heated in the $y$ axis using a single red-detuned 397 nm laser assisted by a resonant 866 nm laser and a proper dc offset driving. For heating the motion in the $y$ direction by a red-detuned laser, five trapped $^{40}Ca^{+}$ ion crystals are deliberately pushed away along the $x$ direction by a dc offset driving for about 10 $\mu$m. This displacement due to driving excites excess micromotion sideband transitions for the motion along the $y$ direction because the micromotion excitation is along the ac electric field, perpendicular to the displaced direction of the ions [16]. As a result, although it provides energy damping and yields cooling in the $x$ and $z$ axes, the properly red-detuned 397 nm laser may play the role of heating in the $y$ axis [17,18] by transferring the excitation from the micromotion to the secular motion. The total effect of the heating can be further understood later from the negative damping in the equation of motion in the $y$ axis (see Appendix A) [19]. Due to the independence of the two kinds of phonons, the micromotion phonons would not interfere with the secular motion phonons outputted as the phonon lasing.

The oscillation amplitude $y_0$ in the $y$ direction is governed by the following equation (see Appendix A for details on the

*liangchen@wipm.ac.cn
†mangfeng@wipm.ac.cn

 

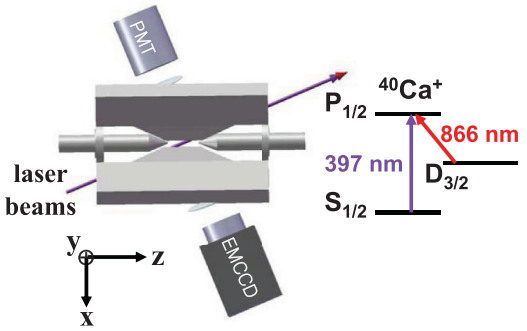


FIG. 1. (Color online) Schematic diagram of the experimental setup (top view) and the relevant energy levels of the $^{40}Ca^+$ ion. The $z$ axis is defined as the trap axis. The compensation electrode located along the $x$ axis is not shown in the picture. The laser spots in the trap center are about 60 and 200 $\mu$m for 397 nm (arrows in purple) and 866 nm lasers (arrows in red), respectively. Scattered 397 nm photons are collected by imaging systems and directed to an electron-multiplying CCD (EMCCD) camera and a photomultiplier tube (PMT).

phonon amplification in the $y$ axis):

$$\dot{y_0} = -\tfrac{1}{2}\mu'(\Delta,\beta,y_0)y_0 + \zeta'(t), \qquad (1)$$

where $\mu'(\Delta,\beta,y_0)$ is a complicated function regarding the laser detuning $\Delta$ to the transition frequency of each ion, the micromotion modulation index $\beta$, and the oscillation amplitude $y_0$. The micromotion modulation index $\beta$ is proportional to the displacement of the ions from the trap center and can be adjusted by the dc offset voltage. $\zeta'(t)$ is a cycle-averaged white noise. Under a proper condition, e.g., $\mu'(\Delta,\beta,y_0) < 0$, coherent phonon amplification (or, say, phonon lasing) can be realized.

## III. OBSERVATION OF THE PHONON LASING AND THE PULSED OUTPUT

As shown in Fig. 2, the threshold behavior of the phonon lasing is observed by sweeping the frequency of the 397 nm laser toward the resonance frequency or by increasing the micromotion modulation index. When the laser detuning increases across $-250$ MHz or the dc offset voltage increases across 235 V, the function $\mu'$ turns from positive to negative and the phonons in the $y$ direction turn from damping to amplification. The case of the function $\mu' = 0$ means a saturation that corresponds to the balance between the damping and the amplification. Figure 2 records such saturation in the variation of 397 nm laser frequency and the dc offset voltage. We may find that the amplification behaves as a hysteresis, which is due to the high nonlinearity of $\mu'(\Delta,\beta,y_0)$ with bistable solutions regarding $\Delta$ and $y_0$. Similar hysteresis has been studied both theoretically and experimentally [7,8].

When the saturation amplitude is larger than the transfer threshold, e.g., 32 $\mu$m in Fig. 3, the phonon transfer occurs between the $x$ and $y$ axes, where the oscillation in the $y$ axis drops rapidly (see Fig. 3), and the vibration in the $x$ axis is thereby excited as shown below in our theoretical analysis. As long as the 397 nm laser is on, this generation and transfer of phonons will repeat periodically due to constant heating in the $y$ axis and constant cooling in other directions.

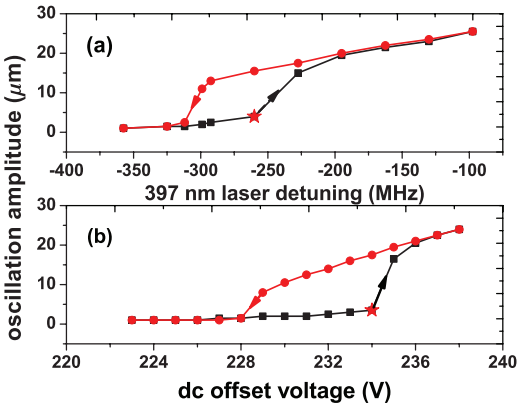


FIG. 2. (Color online) The threshold and amplitude saturation of the phonon lasing. Micromotion modulation is controlled by a dc offset voltage applied on the compensation electrodes, for which 130 V is the optimal value for suppressing the excess micromotion. The arrows in the figure show the sweeping direction. (a) The oscillation amplitude vs 397 nm laser detuning, where the dc offset voltage is 231 V and the laser power is about 35 $\mu$W. (b) The oscillation amplitude vs dc offset voltage, where the 397 nm laser is red-detuned for 280 MHz and the laser power is about 35 $\mu$W. The red stars indicate the threshold points for generating the phonon laser.

Fluorescence is collected during the process above as shown in Fig. 4(a), which can be considered as complementary information to Fig. 3(b). Since the sufficiently long exposure time ($> 0.4$ s) is required for taking an image on EMCCD due to the signal-to-noise ratio in our experiment, which limited the time resolution of the oscillation amplitude measurement, we only present a single measurement point in Fig. 3(b). From

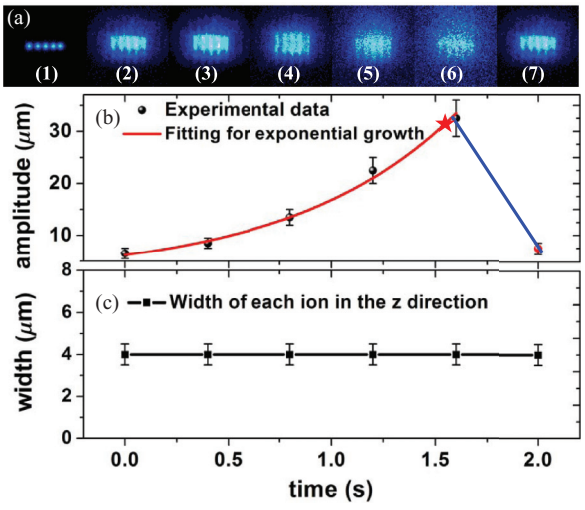


FIG. 3. (Color online) The oscillation amplification and collapse along the $y$ axis. (a) Time-averaged images taken during the process. Each picture is exposed for 0.4 s and the time interval between the successive exposures is 0.01 s. The dc offset voltage is about 270 V and the 397 nm laser is red-detuned by 80 MHz with the power of 15 $\mu$W. The images are as follows: (1) Laser cooling of the ions in both dimensions; (2)–(6) gradual excitation of the ions to larger and larger amplitude oscillation; (7) the amplitude collapsed to a lower value due to phonon transfer to the $x$ axis. (b) The time-stamped amplitude, where the red star indicates the transfer threshold for phonon lasing. (c) The width of the ion crystal in the $z$ axis.

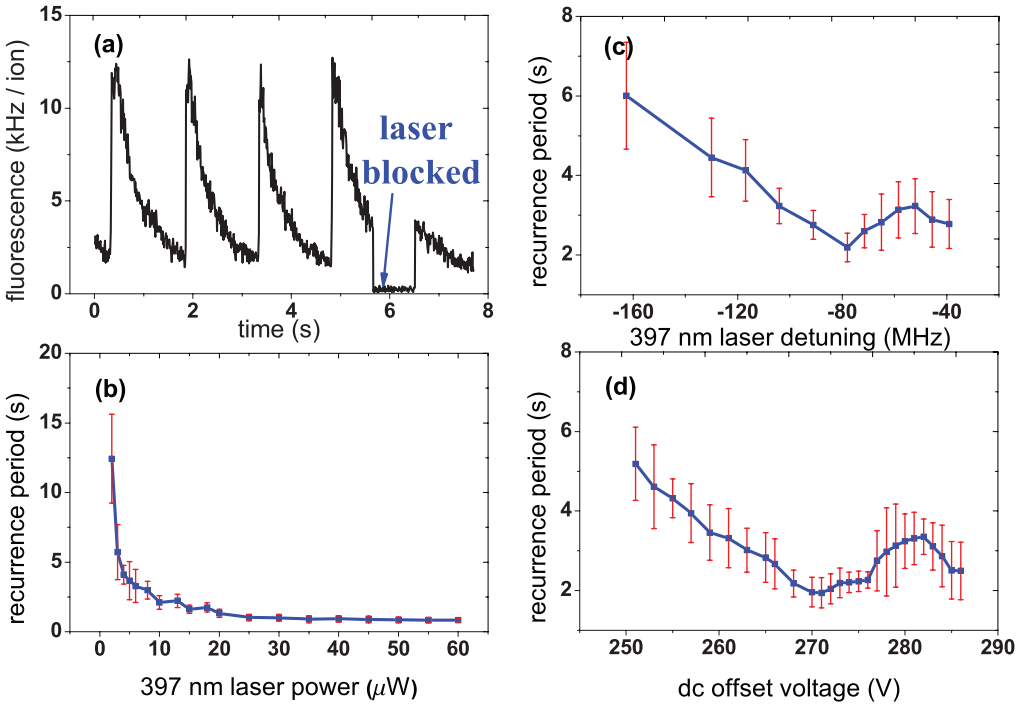


FIG. 4. (Color online) (a) Fluorescence rate signal for 10 ms accumulation during the same process as in Fig. 2, where the arrow points to the collapse due to blockage of the 866 nm laser; (b)–(d) the recurrence periods, averaged by 100 samples, with respect to 397 nm laser detuning and power as well as dc offset voltage, respectively, where (b) the laser detuning $\Delta = -40$ MHz, (c) the laser power $P = 5$ W and the dc offset voltage $V_{\rm dc} = 270$ V, and (d) $\Delta = -70$ MHz and $P = 5$ $\mu$W.

Fig. 4(a), however, we may know more about this process, such as no fast oscillation of fluorescence during the collapse of the oscillation amplitude in the $y$ axis. Moreover, besides the influence from the Doppler shift, the fluorescence rate is also modulated by the oscillation amplitude. Since the oscillation amplitude is comparable to the laser spot and larger than the effective size of the pinhole in front of the PMT, which yields less photon scattering and collection, the larger fluorescence signal corresponds to the smaller oscillation amplitude of the ions. To justify the source of the amplification, we have blocked the 866 nm repumping laser for about 0.8 s during the process of the oscillation amplification. The fluorescence rate drops suddenly and then revives quickly after the blockage is removed, which implies that the excitation of the oscillation is caused by the laser irradiation instead of other factors such as the Coulomb interaction. Moreover, we have also made a series of measurements for the recurrence period under different conditions, which are shown in Figs. 4(b)–4(d).

Due to the fact that the $x$ axis is nearly perpendicular to the imaging plane of the EMCCD in our setup, we have no way to observe the vibration in the $x$ axis directly. But since the width of the ion crystal in the $z$ axis has no obvious expansion during the process of phonon transfer, it is reasonable to conjecture that the excitation of the phonons was transferred to the $x$ axis, which can be clarified further in the following analysis by equations of motion of the ions.

## IV. NONLINEAR COUPLING MODEL AND THE SOLUTIONS

To describe the phonon transfer that occurred in the preceding section, we consider hexapole and octopole anharmonic potentials caused by manufacturing imperfections, which contribute to the nonlinear coupling between the $x$ and $y$ directions [21]. To simplify our treatment, we consider the pseudopotential $U_{\rm eff}(x,y) = \frac{e}{2m}\langle|\int \nabla\Phi(x,y,t)dt|^2\rangle$ [22], and we resort to the effect regarding the micromotion to the damping term in our following treatment. The equations of COM motion for radial directions can be written as

$$\frac{d^2\mathbf{r}}{dt^2} + \frac{e}{m}\nabla U_{\rm eff}(x,y) + \dot{\mathbf{A}}_r - \frac{e\hat{\mathbf{E}}_{\rm dc}}{m} = 0, \qquad (2)$$

where $\mathbf{r} = (x,y)$ is for the position of the ion in different axes, the gradient operator $\nabla$ works in the $x$ and $y$ axes, $\dot{\mathbf{A}}_r = (\hat{\mu}_x\dot{x},\hat{\mu}_y\dot{y})$ is for the laser irradiation effect with $\hat{\mu}_x > 0$ and $\hat{\mu}_y < 0$ representing the damping and amplification, respectively, $\hat{\mathbf{E}}_{\rm dc}$ is the $x$-axial static electric field used for pushing the ions, and $e$ and $m$ are the charge and mass of the ion. As deduced in Appendix B, the equations can be reduced to

$$\ddot{x} + \omega_x^2 x + \hat{\alpha}_3 x^3 + \hat{\alpha}_4 y^2 x + \hat{\mu}_x\dot{x} - \frac{e\hat{E}_{\rm dc}}{m} = 0, \qquad (3)$$

$$\ddot{y} + \omega_y^2 y + \hat{\alpha}_5 y^3 + \hat{\alpha}_7 x^2 y + \hat{\mu}_y\dot{y} = 0, \qquad (4)$$

where $\omega_x$ and $\omega_y$ are the secular frequencies of the radial directions and are slightly different from each other due to the end-cap asymmetry [23]. Parameters $\alpha_3$, $\alpha_4$, $\alpha_5$, and $\alpha_7$ are related to the anharmonic potential, as defined in Appendix B.

Equations (3) and (4) include nonlinearity and intradimensional coupling, which can be solved by the multiple-scale method. Approximate solutions have the form $x = x_0(T_1)\cos[\omega_x T_0 + \theta_x(T_1)]$ and $y = y_0(T_1)\cos[\omega_y T_0 + \theta_y(T_1)]$, where $x_0$ ($y_0$) and $\theta_x$ ($\theta_y$) are amplitudes and phases

of the oscillations in the $x$ ($y$) dimensions, respectively, $T_0$ is a fast time scale associated with the changes occurring at the frequency $\omega_r$, and $T_1$ is a slow time scale. For convenience of treatment, we define $\sigma = 2(\omega_y - \omega_x)$ and $\gamma = \sigma T_1 + 2(\theta_y - \theta_x)$, and we obtain the equations (see details in Appendix B)

$$\begin{aligned}\dot{\gamma} &= \sigma - \frac{3}{8}\left(\frac{\alpha_3}{\omega_x}x_0^2 - \frac{\alpha_5}{\omega_y}y_0^2\right)\\ &\quad -\frac{1}{8}\left(\frac{\alpha_4}{\omega_x}y_0^2 - \frac{\alpha_7}{\omega_y}x_0^2\right)(2+\cos\gamma),\\ \dot{x_0} &= -\frac{\alpha_4}{8\omega_x}y_0^2 x_0 \sin\gamma - \frac{\mu_x x_0}{2},\\ \dot{y_0} &= \frac{\alpha_7}{8\omega_y}x_0^2 y_0 \sin\gamma - \frac{\mu_y y_0}{2},\end{aligned} \tag{5}$$

where $\gamma$ is related to the phase difference of the motion between the $x$ and $y$ directions. $\mu_x > 0$ ($\mu_y > 0$) means cooling in the $x$ ($y$) axis, and $\mu_x < 0$ ($\mu_y < 0$) means heating in the $x$ ($y$) axis.

In the case of small amplitudes, e.g., $|\frac{\alpha_4}{8\omega_x}y_0^2 x_0| \ll |\frac{\mu_x x_0}{2}|$ and $|\frac{\alpha_7}{8\omega_y}x_0^2 y_0| \ll |\frac{\mu_y y_0}{2}|$ are satisfied, we have $\dot{x_0} = -\mu_x x_0/2$ and $\dot{y_0} = -\mu_y y_0/2$. For $\mu_x > 0$ and $\mu_y < 0$, oscillation in the $x$ ($y$) direction becomes smaller (larger), which implies that no phonon transfers from the $y$ axis to the $x$ axis. Therefore, the amplification threshold is the point at which $\mu_y$ turns from positive to negative and the amplitude saturates at $\mu_y = 0$, which is the phonon lasing described before.

For larger amplitudes, the phonon transfer happens only in the case of $\dot{\gamma} = 0$, which means a constant $\gamma$. We may call this the condition of phase-difference locking. Substituting this condition into Eq. (5) and considering the condition that both $\omega_x \cong \omega_y = \omega_r$ and $x_0^2 \ll y_0^2$ are satisfied at the beginning of this process, we obtain the expressions for the amplitude threshold:

$$\begin{aligned} y_0^2 &> \max\left\{\frac{8\sigma\omega_r}{\alpha_4 - 3\alpha_5}, \frac{8\sigma\omega_r}{3(\alpha_4-\alpha_5)}\right\}, && \alpha_5 < \alpha_4 < 3\alpha_5,\\ \frac{8\sigma\omega_r}{3(\alpha_4-\alpha_5)} &< y_0^2 < \frac{8\sigma\omega_r}{\alpha_4-3\alpha_5}, && \alpha_4 > \{\alpha_5, 3\alpha_5\}, \sigma > 0,\\ \frac{8\sigma\omega_r}{\alpha_4-3\alpha_5} &< y_0^2 < \frac{8\sigma\omega_r}{3(\alpha_4-\alpha_5)}, && \alpha_4 < \{\alpha_5, 3\alpha_5\}, \sigma < 0. \end{aligned} \tag{6}$$

The equations present clearly that the amplitude threshold for the phonon transfer is relevant to the anharmonic potentials (i.e., the parameters $\alpha_4$ and $\alpha_5$) and the frequency difference $\sigma$. Besides, once the phonon transfer happens, $\sin\gamma$ should be a negative constant, which is the prerequisite of $x_0$ ($y_0$) increasing (decreasing).

Since cooling works in the $x$ axis during the phonon transfer (i.e., $\mu_x > 0$), the successful output of the pulsed phonon lasing from the $y$ axis to the $x$ axis depends on $\dot{x_0} > 0$, implying that $\sin\gamma < 0$ and $|\frac{\alpha_4}{8\omega_x}y_0^2 x_0 \sin\gamma| > |\frac{\mu_x x_0}{2}|$ during the phase-difference locking. So we have another condition for the coherent output threshold,

$$\begin{aligned} y_0^2 &> B_2, && \alpha_5 < \alpha_4 < 3\alpha_5,\\ B_2 &< y_0^2 < B_1 && \text{otherwise}, \end{aligned} \tag{7}$$

where $B_1 = \frac{8\sigma\omega_r(2\alpha_4-3\alpha_5)}{(\alpha_4-3\alpha_5)(\alpha_4-\alpha_5)} + \frac{4\omega_r\sqrt{4\sigma^2\alpha_4^2+\mu_x^2}}{(\alpha_4-3\alpha_5)(\alpha_4-\alpha_5)}$, $B_2 = \frac{8\sigma\omega_r(2\alpha_4-3\alpha_5)}{(\alpha_4-3\alpha_5)(\alpha_4-\alpha_5)} - \frac{4\omega_r\sqrt{4\sigma^2\alpha_4^2+\mu_x^2}}{(\alpha_4-3\alpha_5)(\alpha_4-\alpha_5)}$. This equation presents a more general condition since it can be reduced to Eq. (6) when $\mu_x = 0$. For $\mu_x > 0$, however, there is possibility of no overlap between the two conditions in Eqs. (6) and (7), which means that no phonon amplification in the $x$ axis will happen. In other words, the phonon lasing is available only when both Eqs. (6) and (7) are satisfied.

Once the output threshold is reached, the self-sustained phonon pulse is outputted. The phonons in the $x$ ($y$) dimension increase (decrease) with the rate proportional to $y_0^2$ until Eq. (7) is not satisfied any more. Then the condition for phase-difference locking breaks down, and the phonon excitation in the $x$ direction starts to decay by the laser cooling and meanwhile the phonons in the $y$ direction are excited again by the laser. This begins a new cycle and such a process proceeds periodically. Moreover, once the phonon lasing is generated in the $y$ direction, since the transient relative phase of oscillations between the $x$ and $y$ directions is locked during the phonon amplification in the $x$ axis, the phonon output should also be coherent, which is analogous to the output of the optical laser.

## V. DISCUSSION

The numerical simulation of Eq. (5) is given in Fig. 5, where the phase-locking behavior and the pulsed phonon transfer are shown. Parameters for the simulation are chosen according to our experimental conditions. The phonon increase in the $x$ axis shows a sharp pulse style when the oscillation amplitude exceeds the output threshold, and the process repeats regularly.

We discuss below how the recurrence period of the pulsed output depends on the damping rate. To this end, we define

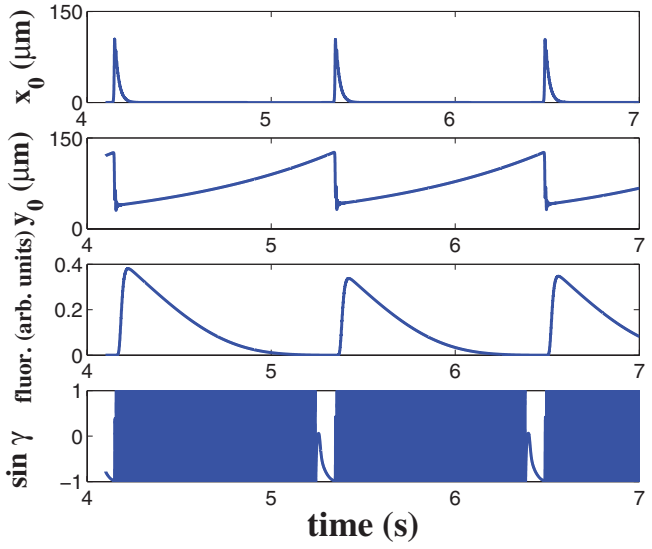


FIG. 5. (Color online) Simulations based on Eq. (5) with the recurrence period 1.2 s. The parameters are set as $\mu_x = 100\ \text{s}^{-1}$, $\mu_y = -2\ \text{s}^{-1}$, $f_1 = 0.05$, and $f_2 = 0.005$ ($f_1$ and $f_2$ are ratios of multipole coefficients in different axes, defined in Appendix B). The fluorescence rate is simulated simply by integrating the laser intensity over the ion trajectory. The bottom plot shows the nearly constant $\gamma$, i.e., the locking of the phase difference.

the kinetic energies of the motion in the $x$ and $y$ directions as $E_x = \frac{1}{2}m\omega_{1x}^2 x_0^2$ and $E_y = \frac{1}{2}m\omega_{1y}^2 y_0^2$, where $\omega_{1x} = \omega_x + \dot{\theta}_x$ and $\omega_{1y} = \omega_y + \dot{\theta}_y$. Our calculation shows that $|\frac{\partial(\dot{E}_x+\dot{E}_y)}{\partial\mu_y}| > |\frac{\partial(\dot{E}_x+\dot{E}_y)}{\partial\mu_x}|$ always holds. This indicates that the energy change and the recurrence frequency are more sensitive to the heating rate $\mu_y$. This is also reflected in the comparison between Figs. 4(c) and 4(d), where there are almost the same curves in both plots with changes of both $\mu_x$ and $\mu_y$ in the former but only the change of $\mu_y$ in the latter.

The better pulsed laser has a narrower pulse width and a higher peak energy. For the pulsed optical laser, this is achieved by $Q$-switching technology, which increases the loss in the amplification stage and decreases the loss in the output stage. For our phonon counterpart, since the loss is attributed to the cooling rate $\mu_x$, an analogous $Q$-switching can also be carried out by controlling $\mu_x$. According to the phonon output condition Eq. (7), if the cooling and amplifying laser beams can be adjusted separately, we may increase $\mu_x$ to enhance the output threshold, yielding more energy accumulation in the amplification stage, and then in the output stage we may decrease $\mu_x$ to enlarge the output rate. Moreover, the recurrence of the phonon lasing pulse can be accelerated by increasing $\mu_y$. So a $Q$-switched pulsed phonon lasing can be built by varying the power of the optical lasers.

## VI. CONCLUSION

In conclusion, pulse-type phonon lasing has been demonstrated for phonon amplification in transverse COM modes of trapped ions. The intradimensional coupling due to hexapole and octupole potentials has been numerically studied using the multiscale method. The phonon laser pulses are generated in the $y$ axis and outputted to the $x$ axis. The micromotion modes are involved but never excited in our experiment, so the single-mode phonon laser output is only related to the secular COM mode. We have also discussed the feasibility of the $Q$-switching technology in our pulsed phonon lasing by separately controlling the cooling and heating of the ions. With highly controllable mechanical motion, engineerable multipole potential [25], and achievable ground-state cooling, the trapped ions can be taken as an ideal platform for studying phonon lasers and nonlinear mechanical oscillators [26].

## ACKNOWLEDGMENTS

This work is supported by the National Fundamental Research Program of China under Grant No. 2012CB922102, and by the National Natural Science Foundation of China under Grants No. 11274352 and No. 11104325.

## APPENDIX A: DETAILS OF THE HEATING IN THE $y$ AXIS

Using the pseudopotential model, the secular COM motion of the ions satisfies the oscillator equation,

$$\ddot{y} + \omega_y^2 y = F_l/m + \zeta(t), \tag{A1}$$

where $F_l$ is the scattering force of the optical laser and $\zeta(t)$ is the white noise including spontaneous emission. For the ions undergoing a large micromotion, the scattering force in the Doppler cooling is frequency modulated by micromotion [17], and we have the equation $F_l/m = -f\dot{y}$, where $f = \frac{2\hbar k^2\Gamma}{m}\frac{\partial\rho_{22}}{\partial\Delta}$ and $\rho_{22} = \frac{\kappa^2}{4}\sum_n \frac{J_n^2(\beta)}{(\Delta - k\dot{y} - n\Omega)^2+\Gamma^2}$, with the natural linewidth $\Gamma$ of the $P_{3/2}$ state, the laser frequency detuning $\Delta$ with respect to the transition frequency of the ion, the micromotion frequency $\Omega$, and $\kappa = \tilde{E}d/\hbar$ with the laser electric field amplitude $\tilde{E}$, the transition electric dipole momentum $d$, the micromotion modulation index $\beta$, and the Bessel function $J_n(\beta)$. So the equation of motion is rewritten as

$$\ddot{y} + \omega_y^2 y = -f(\Delta,\beta,\dot{y})\dot{y} + \zeta(t), \tag{A2}$$

where the function $f$ is strongly relevant to the variables $\Delta$, $\beta$, and $y$. To analyze the motional properties, we suppose the solution as $y = y_0\cos(\omega_y t + \phi)$ with $y_0$ and $\phi$ the amplitude and phase of the slowly varying secular motion (i.e., $\dot{y}_0 \ll y_0\omega_y$ and $\dot{\phi} \ll \omega_y$). Substituting the solution into Eq. (A2) and keeping only leading terms, we obtain

$$\begin{aligned}&\dot{y}_0\sin(\omega_y t+\phi) + y_0\dot{\phi}\cos(\omega_y t+\phi)\\ &= -\frac{1}{2}f(\Delta,\beta,\dot{y})\left\{y_0\sin(\omega_y t+\phi) - \frac{\dot{y}_0}{\omega_y}\cos(\omega_y t+\phi)\right\}\\ &\quad -\frac{1}{2\omega_y}\zeta(t).\end{aligned} \tag{A3}$$

Using the slowly varying nature of $y_0$ and $\phi$ and multiplying the equation by $\sin(\omega_y t + \phi)$, we integrate over one oscillation cycle yielding [8]

$$\dot{y}_0 = -\tfrac{1}{2}\mu'(\Delta,\beta,y_0)y_0 + \zeta'(t), \tag{A4}$$

where $\mu'(\Delta,\beta,y_0) = \frac{1}{\pi}\int_0^{2\pi} d\xi\, f(\Delta,\beta,y_0\omega_y\cos(\xi))\sin^2(\xi)$ and $\zeta'(t) = -\frac{1}{2\pi}\int_t^{t+\tau} dt'\zeta(t')\sin(\omega_y t')$. With the expression of energy $E = m\omega_y^2 y_0^2/2$, we have

$$\dot{E} = -\mu'(\Delta,\beta,E)E + \zeta'(t). \tag{A5}$$

This gives the phonon lasing behavior if $\mu' < 0$ [8], which presents an exponential increase of the energy. It has been proven [17] that the red-detuned laser can provide negative damping (i.e., $\mu' < 0$) and excite the secular motion if the micromotion index is large enough. $\mu'$ is of a very complicated form changing around the value of zero, which makes the dynamics very complicated. The amplitude threshold is set at the point that $\mu'$ turns from positive to negative. The oscillation is saturated when $\mu'$ turns from negative to positive again. This yields the hysteresis.

## APPENDIX B: DETAILS OF THE NONLINEAR COUPLING MODEL

In Cartesian coordinates, a two-dimensional electric potential $\Phi(x,y,t)$ can be expanded as $\Phi(x,y,t) = V(t)\sum_{N=0}^{\infty} A_N\phi_N(x,y)$ [12], where $V(t)$ is the applied rf voltage, $A_N$ is the dimensionless coefficient of the multipole $\phi_N(x,y)$, and the multipole $\phi_N(x,y)$ is of the form $\phi_N(x,y) = \mathrm{Re}[\frac{x+iy}{r_0}]^N$ with $r_0$ a normalization radius. For the multipoles, $\phi_0(x,y)$ represents a constant term with independent $x$ and $y$, $\phi_1(x,y)$ represents the potential from two planes of opposite charges (i.e., a linear dipole), and $\phi_j(x,y)$ with $j = 2,3,4$ are for potentials of quadrupole, hexapole, and octopole, respectively. In our setup, the most relevant potentials are $\phi_j(x,y)$

with $j = 2,3,4$. So the total potential can be expressed as

$$\Phi(x,y,t) = A_2\left(\frac{x^2-y^2}{r_0^2} + f_1\frac{x^3-3xy^2}{r_0^3} + f_2\frac{x^4-6x^2y^2+y^4}{r_0^4}\right), \tag{B1}$$

with $f_1 = \frac{A_3}{A_2}$, $f_2 = \frac{A_4}{A_2}$, and $r_0 = 0.9$ mm for our trap. An effective potential can be derived by averaging the rapid oscillation field $\Phi(x,y,t)$ to be $U_{\rm eff}(x,y) = \frac{e}{2m}\langle|\int \nabla\Phi(x,y,t)dt|^2\rangle$ for a particle with charge $e$ and mass $m$ [22]. Taking into account the laser damping effect as well as the static electric field cause by the compensation electrode, we reach the classical equation of radial motion of the ions in the effective potential $U_{\rm eff}(x,y)$, i.e., Eq. (2).

The equations of motion in the radial directions are written as

$$\begin{aligned} \ddot{x} + \omega_x^2 x + \hat{\alpha}_2 x^2 + \hat{\alpha}_3 x^3 + \hat{\alpha}_4 y^2 x + \hat{\mu}_x \dot{x} - \frac{e\hat{E}_{\rm dc}}{m} = 0, \\ \ddot{y} + \omega_y^2 y + \hat{\alpha}_5 y^3 + \hat{\alpha}_6 xy + \hat{\alpha}_7 x^2 y + \hat{\mu}_y \dot{y} = 0, \end{aligned} \tag{B2}$$

where $\hat{\alpha}_2 = 9f_1\omega_x^2/r_0$, $\hat{\alpha}_3 = (18f_1^2 + 16f_2)\omega_x^2/r_0^2$, $\hat{\alpha}_4 = 18f_1^2\omega_x^2/r_0^2$, $\hat{\alpha}_5 = (18f_1^2 - 16f_2)\omega_y^2/r_0^2$, $\hat{\alpha}_6 = 6f_1\omega_y^2/r_0$, and $\hat{\alpha}_7 = 18f_1^2\omega_y^2/r_0^2$. Since we only consider the near-resonance case $\omega_x \simeq \omega_y$, we may delete the terms of $x^2$ and $xy$ because of their negligible contribution to the dynamics. So Eq. (B2) is reduced to Eqs. (3) and (4) in the main text.

Using the multiple-scale method on Eq. (B2), we have the first-order uniform expansion of the solution [24]

$$\begin{aligned} x &= x_{\epsilon 0}(T_0,T_1) + \epsilon x_{\epsilon 1}(T_0,T_1) + \cdots, \\ y &= y_{\epsilon 0}(T_0,T_1) + \epsilon y_{\epsilon 1}(T_0,T_1) + \cdots, \end{aligned} \tag{B3}$$

where $\epsilon$ is a small dimensionless parameter, $T_0 = t$ is a fast time scale, and $T_1 = \epsilon t$ is a slow time scale. To make use of the perturbative expansion, we scale the nonlinearities and damping coefficients as $\hat{\mu}_i = \epsilon\mu_i$, $i = x,y$, $\hat{\alpha}_n = \epsilon\alpha_m$, $m = 2,\ldots,7$, and $\hat{E}_{\rm dc} = \epsilon E_{\rm dc}$. By substituting Eq. (B3) into Eq. (B2), we have the equations from the coefficients with the same powers of $\epsilon$,

$$D_0^2 x_{\epsilon 0} + \omega_x^2 x_{\epsilon 0} = 0, \quad D_0^2 y_{\epsilon 0} + \omega_y^2 y_{\epsilon 0} = 0 \tag{B4}$$

for the order $\epsilon^0$ with $D_n = \partial/\partial T_n$ $(n = 0,1,\ldots)$, and

$$\begin{aligned} D_0^2 x_{\epsilon 1} + \omega_x^2 x_{\epsilon 1} + 2D_0D_1x_{\epsilon 0} + \alpha_2 x_{\epsilon 0}^2 + \alpha_3 x_{\epsilon 0}^3 \\ + \alpha_4 y_{\epsilon 0}^2 x_{\epsilon 0} + \mu_x D_0 x_{\epsilon 0} - eE_{\rm dc}/m = 0, \end{aligned} \tag{B5}$$

$$\begin{aligned} D_0^2 y_{\epsilon 1} + \omega_y^2 y_{\epsilon 1} + 2D_0D_1y_{\epsilon 0} + \alpha_5 y_{\epsilon 0}^3 \\ + \alpha_6 x_{\epsilon 0} y_{\epsilon 0} + \alpha_7 x_{\epsilon 0}^2 y_{\epsilon 0} + \mu_y D_0 y_{\epsilon 0} = 0 \end{aligned} \tag{B6}$$

for the order of $\epsilon^1$. The general solutions to Eqs. (B5) and (B6) can be supposed as $x_{\epsilon 0} = x_0(T_1)\cos[\omega_x T_0 + \theta_x(T_1)]$ and $y_{\epsilon 0} = y_0(T_1)\cos[\omega_y T_0 + \theta_y(T_1)]$, from which we may eliminate the secular terms regarding $\omega_x$ and $\omega_y$. Then we arrive at Eq. (5).


[1] S. Wallentowitz, W. Vogel, I. Siemers, and P. E. Toschek, Phys. Rev. A **54**, 943 (1996).
[2] I. Bargatin and M. L. Roukes, Phys. Rev. Lett. **91**, 138302 (2003).
[3] E. M. Chudnovsky and D. A. Garanin, Phys. Rev. Lett. **93**, 257205 (2004).
[4] J. Kabuss, A. Carmele, T. Brandes, and A. Knorr, Phys. Rev. Lett. **109**, 054301 (2012).
[5] A. Huynh, N. D. Lanzillotti-Kimura, B. Jusserand, B. Perrin, A. Fainstein, M. F. Pascual-Winter, E. Peronne, and A. Lemaitre, Phys. Rev. Lett. **97**, 115502 (2006).
[6] R. P. Beardsley, A. V. Akimov, M. Henini, and A. J. Kent, Phys. Rev. Lett. **104**, 085501 (2010).
[7] A. E. Kaplan, Opt. Express **17**, 10035 (2009).
[8] K. Vahala, M. Herrmann, S. Knüz, V. Batteiger, G. Saathoff, T. W. Häsch, and Th. Udem, Nat. Phys. **5**, 682 (2009).
[9] S. Knünz, M. Herrmann, V. Batteiger, G. Saathoff, T. W. Hänsch, K. Vahala, and Th. Udem, Phys. Rev. Lett. **105**, 013004 (2010).
[10] M. J. Biercuk, H. Uys, J. W. Britton, A. P. VanDevender, and J. J. Bollinger, Nat. Nanotech. **5**, 646 (2010).
[11] I. Mahboob, K. Nishiguchi, A. Fujiwara, and H. Yamaguchi, Phys. Rev. Lett. **110**, 127202 (2013).
[12] M. Sudakov and D. J. Douglas, Rapid Commun. Mass Spectrom. **17**, 2290 (2003).
[13] C. Marquet, F. Schmidt-Kaler, and D. F. V. James, Appl. Phys. B **76**, 199 (2003).
[14] C. F. Roos, T. Monz, K. Kim, M. Riebe, H. Häffner, D. F. V. James, and R. Blatt, Phys. Rev. A **77**, 040302 (2008).
[15] F. Zhou, Y. Xie, Y. Y. Xu, X. R. Huang, and M. Feng, Chin. Phys. Lett. **27**, 123203 (2010).
[16] D. J. Berkeland, J. D. Miller, J. C. Bergquist, W. M. Itano, and D. J. Wineland, J. Appl. Phys. **83**, 5025 (1998).
[17] R. G. DeVoe, J. Hoffnagle, and R. G. Brewer, Phys. Rev. A **39**, 4362 (1989).
[18] R. Blümel, C. Kappler, W. Quint, and H. Walther, Phys. Rev. A **40**, 808 (1989).
[19] Although it is fully described by classical mechanics, this effect can be also understood in a quantum-mechanical picture. The 397 nm laser is blue-detuned to the micromotion sideband, which leads to absorption of the micromotion phonons and at the same time emission of secular motion phonons in the $y$ axis [20].
[20] D. Leibfried, R. Blatt, C. Monroe, and D. Wineland, Rev. Mod. Phys. **75**, 281 (2003).
[21] M. Vedel, J. Rocher, M. Knoop, and F. Vedel, Appl. Phys. B **66**, 191 (1998).
[22] A. Doroudi, Phys. Rev. E **80**, 056603 (2009).
[23] A. Drakoudis, M. Sollner, and G. Werth, Int. J. Mass Spectrom. **252**, 61 (2006).
[24] T. A. Nayfeh, W. Asrar, and A. H. Nayfeh, Nonlinear Dyn. **3**, 385 (1992).
[25] M. Sudakov and D. J. Douglas, Rapid Commun. Mass Spectrom. **17**, 2290 (2003).
[26] N. Akerman, S. Kotler, Y. Glickman, Y. Dallal, A. Keselman, and R. Ozeri, Phys. Rev. A **82**, 061402 (2010).